SUBSURFACE IMAGING ANALYSIS FOR MULTIPLE DIELECTRIC OBJECTS BURIED UNDER HOMOGENOUS GROUND

Esin Karpat
Department of Electronics Engineering, Uludag University, Bursa, TURKEY

ABSTRACT

A challenging complex electromagnetic problem, subsurface imaging, requires reliable sensor configurations and effective signal processing algorithms. Problems vary from medical diagnosis (e.g., tumor detection) to the military applications (location of buried land mines, underground explosives, hidden headquarters, etc.). Investigations on improving imaging quality have focused on better antenna system design, signal waveform exploration, sensor integration, and intelligent signal processing methods. Numerical simulations in these areas play an important role both in understanding physical background of the problem and in doing research in these challenging areas.

Recently developed finite-difference time-domain (FDTD) method based on two-dimensional virtual, GrGPR, can be used in simulations of variety of subsurface problems. In this paper, GrGPR is used for synthetic data generation for the direct problem. Synthetic aperture type antenna array configuration with different time-domain signal waveforms is reviewed. Finally, Subsurface Imaging (SSI) capabilities for multiple dielectric objects buried under homogenous dielectric ground are summarized as an inverse problem for different waveforms, frequencies and dielectric properties.

KEYWORDS: *FDTD, ground penetrating radar (GPR), image reconstruction, microwave imaging, mine detection, object identification, sensor scan, subsurface imaging, synthetic aperture radar, tumor detection*

I. INTRODUCTION

Subsurface imaging is one of the challenging complex electromagnetic problems with various applications in military and biomedical areas which have great importance for human life. The high dielectric contrast between malignant tumors and surrounding lesion-free normal breast tissues and the translucency of the breast tissue to microwaves have been encouraging the use of microwave energy for the detection of breast cancer [1-10]. The studies on subsurface imaging in military area depend on the detection of deadly targets such as land mines and unexploded ordnance [12-20].

Since the medium, where the scatterers are buried, is not homogenous and refractions occur due to boundary-layer interface, problems related to constructing subsurface images is more severe than that of forming the radar images in the free-space. Therefore this complex problem requires a reliable sensor or multi-sensors, better waveforms, and effective signal processing algorithms.

One way to investigate all these aspects is to use numerical simulation methods. Finite-difference time-domain (FDTD) method has been widely used in subsurface imaging problems [1-4, 12, 16, 17, 19, 22-25].

In this paper, synthetic data for the direct scattering problem are generated by recently introduced FDTD-based subsurface imaging virtual tool, GrGPR. In the second section of the paper the virtual

tool GrGPR is introduced. Scattering data for various scenarios are recorded for both Linear FM (chirp) and Gauss waveforms. In the third part the signal waveforms LFM and Gauss are discussed. The steps for 2D image reconstruction are examined in the fourth section and the results are given in the fifth section subsurface imaging capabilities are summarized for various simulation parameters.

II. FDTD-BASED VIRTUAL SUBSURFACE IMAGING TOOL-GRGPR

The GrGPR is a general purpose EM tool. Figure 1 shows its front-panel and user-created typical scenarios. The main simulation window is a 700x350 cell FDTD computation space terminated by simple MUR-type boundary blocks. The top blocks are reserved for user-specified operational parameters and run-time commands. The physical size of the space is specified from upper-left-block. The frequency or bandwidth is calculated automatically according to Courant stability criteria [12]. Any of four boundaries from left, right, top, and bottom can be set to reflecting or non-reflecting (free-space) termination. Triangular, rectangular, and/or elliptical objects, either perfectly electrical conductor (PEC) or lossy, can be located by just selecting an object and clicking/dragging the mouse. A flat or irregular lossy ground with buried objects may also be generated. The irregular terrain is produced automatically using cubic-spline interpolation algorithm once the user locate a number of points and filling the area between the curve and the bottom (left mouse button) or top (right mouse button) boundary. Another block is reserved for the excitation. A continuous wave (CW), a Gaussian or a rectangular pulse, or a chirp signal can be generated. As many as N radiators/receivers can be located either in pair or alone (here, N is set to 100).

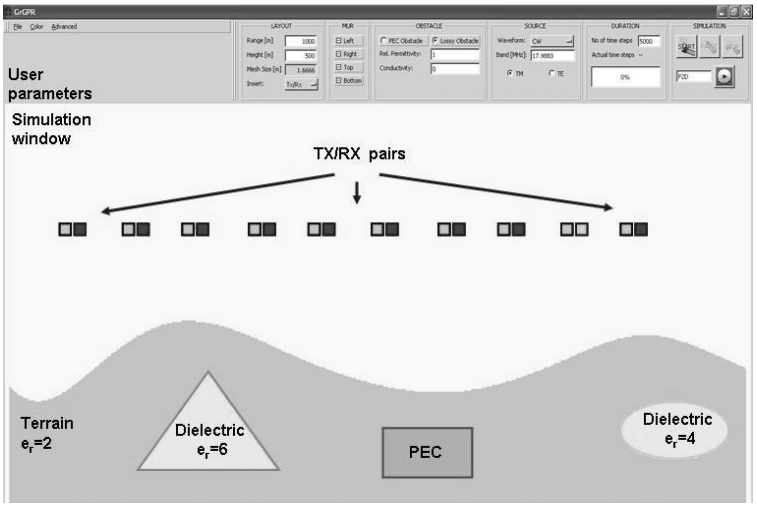

Figure 1. The front panel of 2D FDTD-based GrGPR virtual tool and user-created typical scenario.

Radiators/receivers can be grouped as linear, triangular, rectangular or elliptic arrays. Different excitations can be applied. The radiator/ receiver elements can be activated at the same time (i.e., beam forming), or a time delay can be applied consecutively (i.e., activated sequentially) to form a SAR-type illumination. The number of transmitters and receivers, inter-element distance and time delay, may be specified from Advanced/Source menu. Finally, the two blocks on the top-right are reserved for operational buttons and parameters. Time simulations may also be recorded as EM video clips.

III. COMPARISON OF LINEAR FM (CHIRP) AND GAUSS SIGNAL

Linear FM (LFM) pulse (1), also known as chirp pulse, is one of the best functions to achieve better range resolution which is an important point for detection of scatterers closed to each other, (*T;* pulse duration, f_c; initial frequency, *a;* the rate of frequency change (chirp rate)).

$$s(t) = \cos(2\pi(f_c t + 0.5at^2))rect((t - T/2)/T) \quad (1)$$

In microwave imaging, the range resolution of the pulsed radar is calculated as

$$\Delta R = \frac{v_p T}{2} \tag{2}$$

where v_p is the phase velocity of waves and T is the pulse duration. If the distance between scatterers is less than range resolution the return pulses will overlap. Since keeping the pulse duration less will also decrease the energy transmitted which is not a suitable for detection of scatterers far away from the transmitters. Hence an alternative is to design a pulse shape that has sufficiently short time duration while having the required energy and may be processed to distinguish different scatterers.

In this study linear FM pulses are generated by selecting an initial frequency and increasing or decreasing the frequency value within a specified frequency range and time steps. Since the bandwidth of the pulse will change proportional to *a (B=aT)*, then the range resolution will be

$$\Delta R = \frac{v_p}{2B} = \frac{v_p T}{2aT^2} = \frac{v_p T}{2aT^2} \tag{3}$$

The resolution of LFM signal can further be enhanced by the compression of chirp pulse through matched filtration (Figure 2) [6]. The matched filtration can be performed either as a convolution in the time domain or as a direct multiplication in the frequency domain. The latter requires FFT and IFFT processes. Then processed data and round-trip delays of the transmitter-pixel-receiver are used to reconstruct the image. The simulation results are compared with those images reconstructed with Gaussian signal.

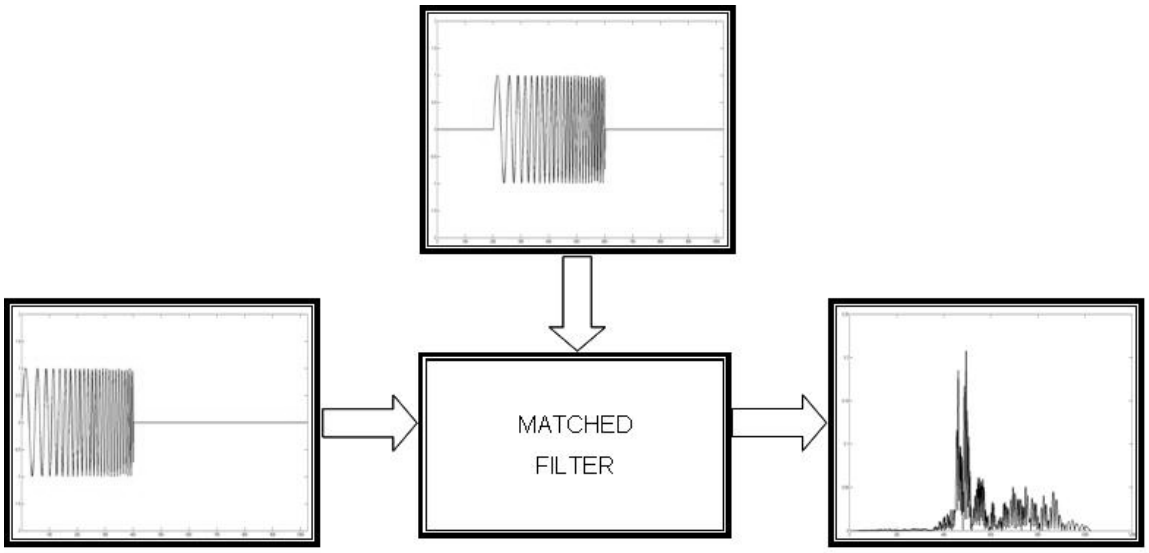

Figure 2. Range compression by matched filter

IV. GENERATING 2D IMAGES

4.1. Subsurface Scenarios and Synthetic Data Collection

Data needed to generate 3D images are collected via GrGPR, a finite-difference time domain (FDTD) method based virtual tool, [24]. Different subsurface scenarios can be generated with this simulation package. An example of these scenarios is shown in Figure 3. Two elliptical dielectric objects are buried under a loss-free layer which has a relative permittivity (ε_r) of 2. Fifty TX/RX antenna pairs are located above the plain ground.

The antenna pairs are activated consecutively as in SAR type scanning scenarios. The signals, generated and received by each TX/RX pairs are saved for post-processing. By activating each antenna pair at a time, N (number of antenna pairs) vectors with Mx1 dimension are collected. M is the number of time steps which should be enough to let all scattered transient fields are recorded with the receivers.

The received raw signals consist of both the early-time and late-time responses. The early-time response consists of the outgoing signal shot by an antenna and also the signal reflected from the ground layer and is orders of larger than the backscatter signal from the scatterer. Even though in the literature, there are several methods to get rid of the early time signal [2-4, 7, 17, 19-25], in this study repeating the FDTD simulation in the absence of scatterer is preferred. So the received signals in the absence of scatterer can be subtracted from the raw signals to obtain the signal scattered from object [6].

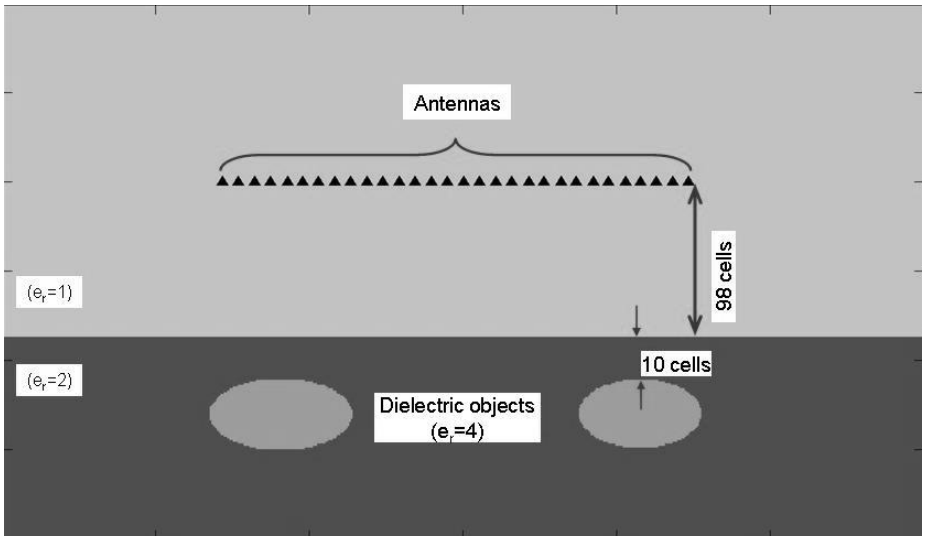

Figure 3. A subsurface imaging scenario with an eliptical dielectric object buried under loss free ground layer with relative permittivity 2.

4.2. Reconstruction of Subsurface 2D Images and SSI Algorithm

The Subsurface Imaging (SSI) algorithm has recently been introduced [24]. The accumulation of late-time responses from every single cell to a pair of radiator/receiver necessitates the calculation of round-trip signal delay. Denote coordinates of each cell/pixel by (x_i,y_j), where x and y are the horizontal and vertical axes, respectively. Coordinates of the k^{th} radiator/receiver pair is denoted by (x_t^k, y_t^k).The time necessary for a round-trip from the radiator to the cell/pixel, and back to the receiver can then be calculated via

$$\tau_{i,j}^k = \frac{2*\sqrt{(x_i - x_t^k)^2 + (y_j - y_t^k)^2}}{\upsilon_p} \tag{4}$$

where υ_p is the phase velocity and it is equal to c, speed of light, for free space. It must be noted that, round-trip delays calculated from (4) must be replaced by an expression which takes into account Snell's Law if an object buried under the homogenous ground is of interest [14], (Figure 4). The pixels (x_{int},y_{int}) where the propagating wave intersects with the surface can be obtained through Snell's law (5).

$$n_1 \sin\theta_1 = n_2 \sin\theta_2 \tag{5a}$$

$$n = \sqrt{\varepsilon\mu} \tag{5b}$$

$$\sqrt{\varepsilon_1}\frac{\left|\left(x - x_t^k\right)\right|}{\sqrt{\left(x - x_t^k\right)^2 + (y - y_t^k)^2}} - \sqrt{\varepsilon_2}\frac{\left|\left(x - x_i\right)\right|}{\sqrt{\left(x - x_i\right)^2 + (y - y_j)^2}} = 0 \tag{5c}$$

The time necessary to reach the intersection cell on the surface of the ground and from surface to the corresponding pixel must be calculated individually (6).

$$\tau_{1(i,j)}^{k} = \left(\frac{\sqrt{\left(x_{int} - x_t^k\right)^2 + \left(y_{int} - y_t^k\right)^2}}{c} \right) \tag{6a}$$

$$\tau_{2(i,j)}^{k} = \frac{\sqrt{\left(x_{int} - x_i\right)^2 + \left(y_{int} - y_j\right)}}{v_p} \tag{6b}$$

$$\tau_{(i,j)}^{k} = 2*\left(\tau_{1(i,j)}^{k} + \tau_{2(i,j)}^{k}\right) \tag{6c}$$

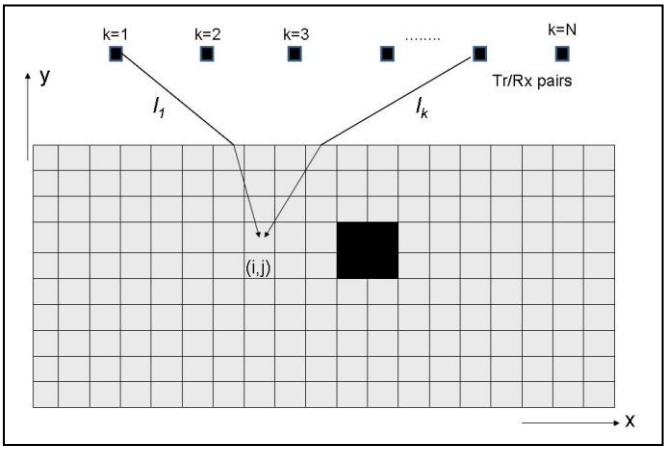

Figure 4. The refraction of ray paths on the surface of homogenous ground.

The corresponding pixel (distance) index can then be obtained from

$$l_{i,j}^{k} = \frac{\tau_{i,j}^{k}}{\Delta t} \tag{7}$$

where Δt is the FDTD time step. The field intensity of each cell (i.e., the image color) is then formed as

$$I(i,j) = \sum_{k=1}^{N} a_{i,j}^{k}(l_{i,j}^{k}) \tag{8}$$

where $a_{i,j}^{k}$ is the intensity at $l_{i,j}^{k}$ Figure 5 shows the block diagram of the SSI algorithm.

In summary, the three step SSI algorithm is based on the calculation of the time delays of all roundtrips from all pixels to all scan points, noise/clutter elimination and signal enhancement (i.e., matched filtration), and superposing scattered field values corresponding to those delays.

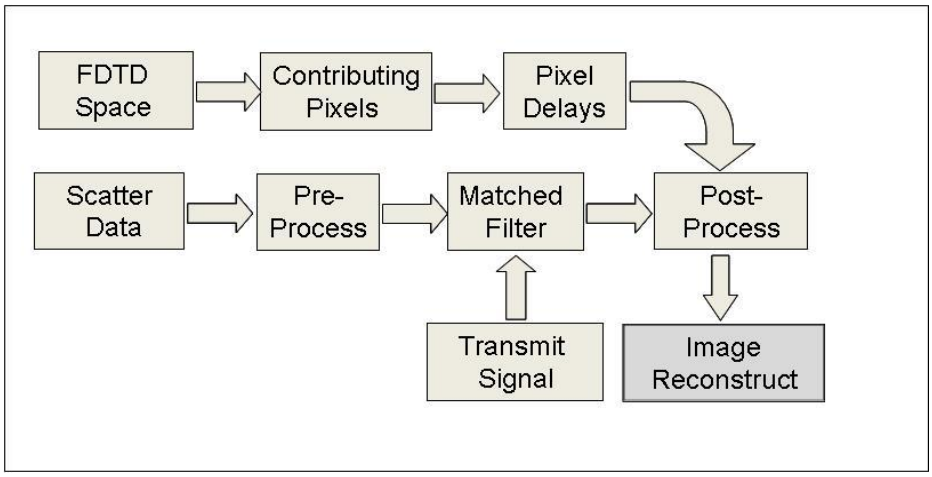

Figure 5. The block diagram of the presented SSI algorithm [24].

V. RESULTS AND DISCUSSION

Various SSI scenarios are created using the GrGPR tool and scattered time data are recorded. The images are reconstructed via the SSI algorithm. The dimensions of the 2D xy-simulation space are set to 1000 m x 500 m. The total number of FDTD time steps is set to 2048. All examples presented here are run for a Gaussian with a frequency of 2 GHz and LFM (chirp) UWB pulse with frequency swept from 500MHz to 2 GHz in 400 time steps. The transmit/receive antenna pair is located at 50 different points above the ground under investigation and activated sequentially to perform a SAR scan. All objects presented below are dielectric. The results are obtained for various dielectric properties.
Gauss signal with frequencies 17 MHz, 1 GHz and 2 GHz is transmitted to obtain synthetic data. Figure 6 shows 2D images obtained by using Gauss and Chirp signals. The reconstructed images are compared with the results for chirp signal (500Hz-2GHz) (Figure 6). It is seen that chirp signal gives more clear results as compared to Gauss signal.

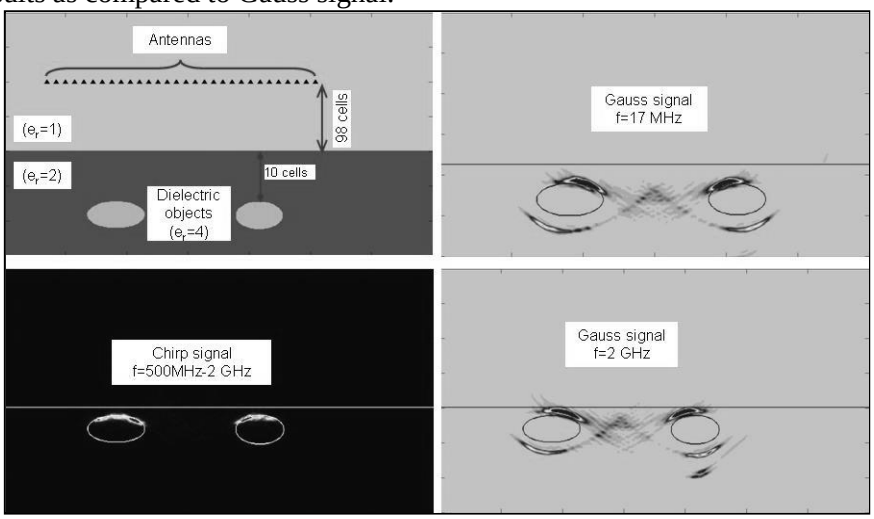

Figure 6. Two dielectric (e_r=4) objects buried under dielectric (e_r=2) homogenous ground (top-left), 2D images obtained with Gauss signal with 17 MHz frequency (top-right), 2 GHz frequency (bottom-right), Chirp signal with 500MHz-2GHz frequency range (Bottom-right).

To compare how the frequency effect the reconstruction of images, two dielectric objects are buried under 80 Yee cells below dielectric (er=2) homogenous ground. 2D images are obtained by transmitting 1, GHz, 2 GHz Gauss signal and 500MHz-1,5GHz and 500MHz-2GHz chirp signal, (Figure 7, left column and right column, respectively). It is observed that the higher frequencies give more clear images when compared to lower frequencies.

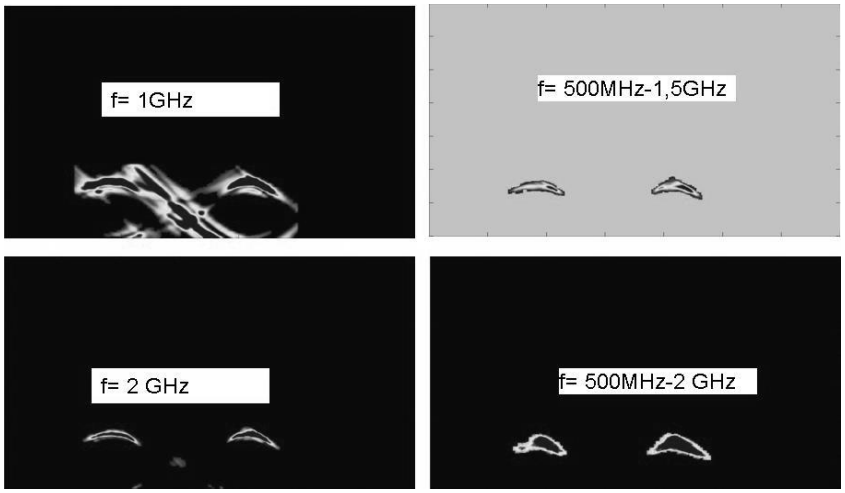

Figure 7. Two dielectric (e_r=6) objects buried under 80 Yee cells below dielectric (er=2) homogenous ground. 2D image obtained with Gauss signal of 1 GHz (top-left) and 2 GHz (bottom-left) and LFM signal 500MHz-1,5GHz (top-right) and 500MHz-2 GHz (bottom-right).

To examine the effect of dielectric properties of buried objects, two dielectric objects are buried under 80 Yee cells below dielectric (e_r=2) homogenous ground. 2D images are obtained by transmitting 2 GHz Gauss signal and 500MHz-2GHz chirp signal on the left and right column, respectively. The simulations are repeated for the objects with different dielectric permittivity. The relative permittivity of the objects changes as 4, 6, and 9, top, middle and bottom, respectively (Figure 8).
Note that, tests with arbitrary shaped PEC and dielectric multi-objects should extensively be done in order to draw conclusions about SSI approach discussed here. Only after then, this approach and developed SSI algorithms can be used to monitor reliably.

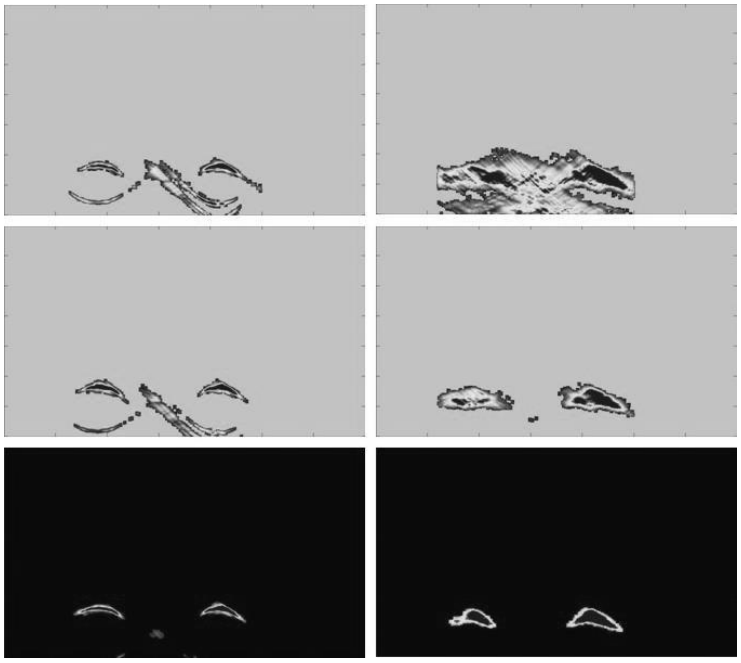

Figure 8. Two dielectric objects buried under 80 Yee cells below dielectric (er=2) homogenous ground. 2D images are obtained with both Gauss (2GHz, (left)) and Chirp signal (500MHz-2GHz, (right)) for objects with different dielectric properties (e_r=4 (top), 6 (middle), 9(bottom)).

VI. CONCLUSIONS

Subsurface imaging and reconstruction is discussed in 2D idealized environments and attention is paid to various signal waveforms and object properties. A recently introduced FDTD-based GrGPR virtual tool is used and forward scattered data is generated synthetically. SSI algorithm is used to reconstruct 2D images. The dielectric properties of buried objects, signal types and signal frequency are analysed as independent parameters towards finding optimum conditions.

The results show that as the dielectric constant of the objects increase the penetration depth of the material and the internal reflections/scattering decrease. So the contour of the object is obtained more clearly. The range compression advantage of the LFM signal also give the opportunity to obtain more clear images than gauss signal.

VII. FUTURE WORK

Subsurface imaging is a challenging complex electromagnetic problem on which extensive research is still required. The present stage of the GrGPR is appropriate for 2D simulations. The simulations and the image processing algorithms give good results for 2D scenarios. For more realistic scenarios, virtual tool and processing algorithms will be expanded for 3D simulations.

REFERENCES

[1] B. Guo, Y. Wang, J. Li, P. Stoica, and R. Wu, "Microwave imaging via adaptive beamforming methods for breast cancer detection", Progress In Electromagnetics Research Symposium 2005, Hangzhou, China, August 22-26.

[2] E. J. Bond, X. Li, S. Hagness, B. Van. Veen, " Microwave imaging via space-time beamforming for early detection of breast cancer", IEEE Transaction on Antennas and Propagation, Vol. 51, No. 8, pp. 1690-1705, August 2003.

[3] X. Li, S. C. Hagness , "A confocal microwave imaging for breast cancer detection", IEEE Microwave and Wireless Components Letters, vol. 11, no. 3, pp. 130-132, Mar. 2001.

[4] E. C. Fear, X. Li, S. C. Hagness, M. A. Stuchly, "Confocal microwave imaging for breast cancer detection: localization of tumors in three dimensions", IEEE Transactions on Biomedical Engineering, vol. 49, no. 8, pp. 812-822, Aug 2002.

[5] E. C. Fear, P. M. Meaney, M. A. Stuchly, "Microwaves for breast cancer detection?", IEEE Potentials, pp.12-18, Feb/Mar 2003.

[6] P.R.P. Hoole, P. D. Oxon, (Eds) "Smart antennas and signal processing for communications, biomedical and radar systems", WIT Press, Ashurst, England, (T. P. Hua, D. Goh, P.R.P. Hoole, U. R. Abeyratne, Ch 6; pp. 191-220), 2001.

[7] T. C. Williams, E. C. Fear, D. T. Westwick, "Tissue sensing adaptive radar for breast cancer detection-investigations of an improved skin-sensing method" , IEEE Trans. MTT, vol. 54, no. 4, pp. 1308-1314, April. 2006.

[8] Mohammed, Beada'a J.; Abbosh, Amin M.; Sharpe, Philip, "Planar array of corrugated tapered slot antennas for ultrawideband biomedical microwave imaging system" International Journal of RF and Microwave Computer-Aided Engineering, vol. 23, no: 1, pp: 59-66, doi: 10.1002/mmce.20651, Jan. 2013.

[9] Nikolova, N.K. ,"Microwave Imaging for Breast Cancer", IEEE Microwave Magazine, vol. 12 , no:7, pp: 78 – 94, Dec.,2011.

[10] Chen, Y.; Kosmas, P. ,"Microwave Breast Tumor Sensing and Targeting Using Multiswarm Contrast-Agent-Loaded Bacterial Nanorobots", International Conference on Electromagnetics in Advanced Applications (ICEAA) / IEEE-APS Topical Conference on Antennas and Propagation in Wireless Communications (IEEE APWC) / URSI Electromagnetic Environment and Interference Symposium (EEIS), Cape Town, South Africa, Sep. 02-07, 2012.

[11] Ahmad, S. W.; Chen, Y. ,"Feasibility Study of Tumor Morphology Classification via Contrast-Enhanced UWB Breast Imaging - A Pole-Zero Analysis", International Conference on Electromagnetics in Advanced Applications (ICEAA) / IEEE-APS Topical Conference on Antennas and Propagation in Wireless Communications (IEEE APWC) / URSI Electromagnetic Environment and Interference Symposium (EEIS), Cape Town, South Africa, Sep. 02-07, 2012.

[12] K. S. Yee, "Numerical Solution of Initial Boundary Value Problems Involving Maxwell's Equations in Isotropic Media" , IEEE Transactions on Antennas and Propagation, vol. 14, no. 5, May 1966, pp. 302 – 307.
[13] H.B.D. Sorensen, K.B. Jakobsen, O. Nymann, "Identification of mine-shaped objects based on an efficient phase stepped-frequency radar approach", 1997 International Conference on Image Processing (ICIP'97) , vol. 3, pp.142, 1997.
[14] L. Wentai, Su Yi,,"A UWB impulse subsurface imaging radar", 2005 IEEE International Symposium on Microwave, Antenna, Propagation and EMC Technologies for Wireless Communication Proceedings, pp. 1356-1360, 2005.
[15] L. Peters Jr, J. J. Daniels, J. D. Young, "Ground penetrating radar as a subsurface environmental sensing tool", Proceedings of. the IEEE, vol. 82, no. 12, pp.1802-10822, Dec. 1994.
[16] L. Gürel, U. Oğuz, "Simulations of ground-penetrating radars over lossy and heterogeneous grounds", IEEE Trans on Geosci. and Remote Sensing, vol 39, no. 6, pp. 1190-1197, June 2001.
[17] R.Nilavalan, G.S.Hilton and R.Benjamin, "A FDTD model for the post-reception synthetic focusing surface penetrating radar with mine detecting applications", National Conference on Antennas and Propagation: 30 March - 1 April 1999, Conference Publication No. 461, pp.69-72, IEE, 1999.
[18] R. J Chignell, "Ground penetrating radar - A sensor for mine detection", "Detection of abandoned land mines", The Detection of Abandoned Land Mines: A Humanitarian Imperative Seeking a Technical Solution, EUREL International Conference on, 7-9 October 1996, no. 431, pp. 103-108, IEE 1996.
[19] U. Oğuz, L. Gürel, "Modeling of ground-penetrating-radar antennas with shields and simulated absorbers", IEEE Trans on Antennas and Propagat., vol 49, no.11, pp.1560-1567, Nov. 2001.
[20] Xu Li, Essex J. Bond, B. Van Veen, Susan Hagness, "An overview of UWB microwave imaging via space-time beamforming", IEEE Antennas and Propagation Magazine, vol. 47, no.1 Feb., 2005.
[21] Y. Wang, X. Li, y. Sun, J. Li, P. Stoica, "Adaptive imaging for forward-looking ground penetrating radar," IEEE Trans. Aerospace And Electronic Systems, vol. 41, no. 3, pp.922-936, Jul 2005.
[22] F. Akleman, M.O. Özyalçın, L.Sevgi, "Subsurface imaging and time domain numerical simulation techniques", Progress in Electromagnetics Research Symposium (PIERS 2002) (invited paper for special "Subsurface Imaging and Reconstruction" session), July 1-5, 2002, Boston, USA.
[23] G. Çakır, L. Sevgi, M. Çakır, "A multipurpose FDTD-based two dimensional electromagnetic virtual tool", IEEE Antennas and Propagation Magazine, vol. 48, no.4, pp.142-151, Aug 2006.
[24] E. Karpat, M. Çakır, L. Sevgi, "Subsurface imaging, FDTD-based simulations and alternative scan/processing approaches", Microwave and Optical Technology Letters, vol. 51, no.4, pp.1070-1075, April 2009.
[25] E. Karpat, "CLEAN Technique to classify and detect targets in subsurface imaging", International Journal of Antennas and Propagation, (in press, 2012), doi: 10.1155/2012/917248.

AUTHOR

Esin Karpat received her B.S.E.E., M.S.E.E. and Ph.D. degrees in Electronics Engineering from Uludag University (UU) in 1996, 2002, and 2009, respectively. In 2000 she joined UU as a research assistant. In 2006, while working on her Ph.D. she had been at Texas Tech University, USA, for one year, for her PhD research. Dr. Kapat, is still with Electronics Engineering Department as a research assistant.